SMART ANTENNAS IN UMTS LCR-TDD
Implementation of RSS Beamforming

Arjang Hessamian-Alinejad, Achim Seebens, Tobias Scholand, Admir Burnic,
Guido H. Bruck and Peter Jung

Lehrstuhl für KommunikationsTechnik, Universität Duisburg-Essen, 47048 Duisburg, Germany

Keywords: Beamforming, DSP (Digital Signal Processor), LCR-TDD (Low Chip-Rate Time Division Duplex), Regular Spatial Sampling (RSS) Smart Antennas, UMTS (Universal Mobile Telecommunications System).

Abstract: In this communication a novel beamforming scheme is presented, which is based on regular spatial sampling (RSS) of signals. RSS beamforming allows low-complexity algorithms for smart antennas, while at the same time improving the performance of those systems. An implementation concept is presented, which shows the feasibility of implementing RSS beamforming on today's readily available hardware platforms.

1 INTRODUCTION

In the LCR-TDD (Low Chip-Rate Time Division Duplex) mode of UMTS (Universal Mobile Telecommunications System), the application of smart antennas is anticipated (Holma et al., 2002). A smart antenna is the combination of an array antenna with an appropriate signal processing algorithm, which is applied to the signals coming from or going to the antenna elements of the array antenna (Lehne et al., 1999), (Correia,2001). Smart antenna concepts range from simple switching between directive antenna elements of an array antenna to highly-sophisticated adaptive beamforming techniques, which aim to maximize the signal-to-interference-and-noise ratio (SINR) for the user of interest during reception, while in the transmit direction reducing the interference to other users as far as possible (Lehne et al., 1999). Beamforming can be viewed as spatial filtering by adjusting the beam pattern of the array antenna through the application of beamforming weights to the signals of the antenna elements.

Here, we will focus on receiver beamforming. The majority of beamforming concepts apply array antennas with K_a identical wired antenna elements, making the analysis and design of the array antenna very simple. In order to avoid large unwanted side lobes the antenna spacing must not be larger than $\lambda/2$, where λ is the wavelength of the radio signals in mind. However, placing the antenna elements too close increases the coupling between the antenna elements and broadens the minimum achievable beam width. Hence, in most arrays the antenna element spacing is $\lambda/2$.

First the general concepts of conventional and the novel Regular Spatial Sampling (RSS) beamforming shall be considered. In figure 1, a scenario consisting of three user signals impinging from the Directions Of Arrival (DOA) $\beta = 60°$, $\beta = 120°$, and $\beta = 240°$, onto an array antenna is shown. The array antenna is a UCA consisting of $K_a = 4$ antenna elements with an antenna element spacing of $\lambda/2$. The conventional beamformer expresses a single beam for each impinging wave, which are shown in figure 1 in blue, magenta and red for the signals impinging from $\beta = 60°$, $\beta = 120°$, and $\beta = 240°$, respectively. Looking at the blue beam steered in the direction $\beta = 60°$ this beam not only receives the user of interest, but also due to its side lobes the other two impinging signals. These are considered as interference in the conventional beamformer. Likewise it is for the other two impinging signals.

The conventional beamformer can be viewed as a spatial matched filter as it maximizes the signal-to-noise ratio (SNR) in the receiver. However, since the beamformer steers the beam into the directions of the impinging signals, these directions have to be estimated. Appropriate DOA algorithms like e.g.

ESPRIT (Paulraj et al., 1986) can become computationally very complex.

The expression of beams into the DOAs of the impinging signals can be seen as sampling the space. As can be seen from the above discussion this is an irregular spatial sampling, since the beams are directed into the DOAs of the impinging waves, which may be any directions. From the processing of time domain signals it is known that processing of irregularly sampled signals is often more complex than the processing of regularly sampled signals. This is the main idea of the novel RSS beamforming technique, which represents a regular sampling of the space (Seebens et al., 2004), (Scholand et al., 2004).
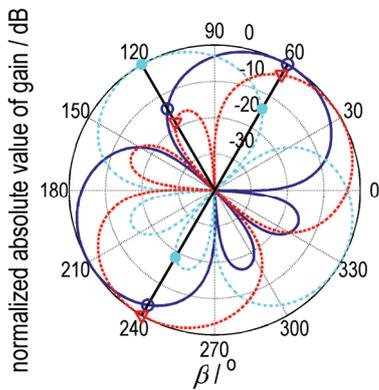
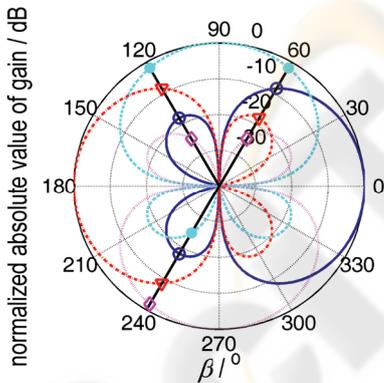

Figure 1: Conventional beamforming.

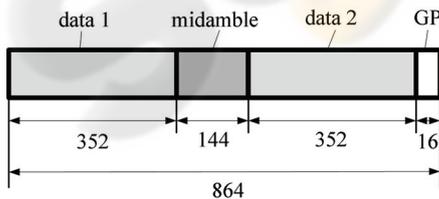Figure 2: Regular spatial sampling (RSS) beamforming.

Figure 3: Burst structure for the LCR-TDD mode of the UMTS system (3GPP TS 25.221 V5.2.0, 2002).
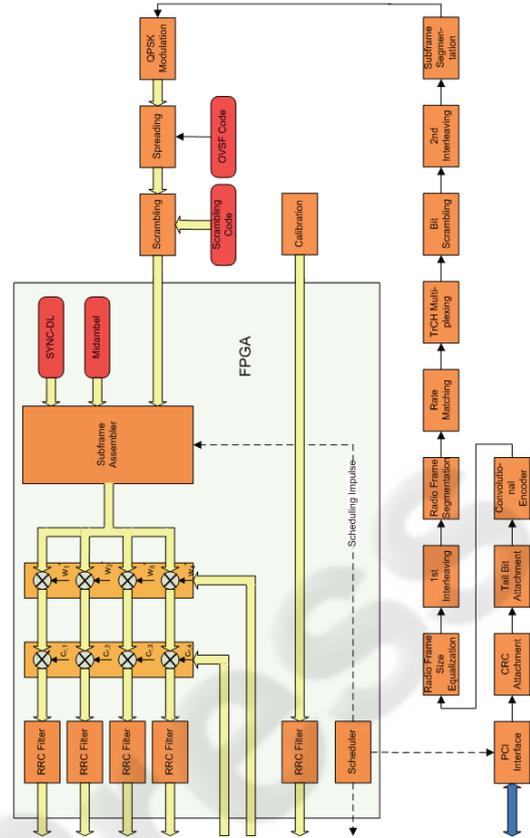

Figure 4: Block diagram for the Node B transmitter.

Figure 2 shows the concept of RSS beamforming for the same scenario as above for the conventional beamforming. Contrary to conventional beamforming the number of expressed beams does not depend on the number of users. Instead a fixed number of beams is expressed, which is suitable to sample the space. For the circular array with $K_a = 4$ antenna elements like the one for the conventional beamformer there are four independent beams possible, shown in figure 2 in blue, magenta, red and violet for the directions $0°$, $90°$, $180°$, and $270°$, respectively. Because of the beam width and the side lobes of the beams each beam naturally receives signals from more than one direction. These are not considered as interference as in the conventional beamforming concept, but contribute to the overall received energy due to maximum ratio combining schemes. Since the RSS beamformer directs its beams into predetermined directions it can totally renounce on DOA estimation techniques. This allows a low-complexity beamformer with very good performance.

In this communication the performance of the RSS beamforming concept is investigated with respect to

the LCR-TDD mode of UMTS. Especially, simulation results are shown with a promising performance. An implementation concept for a demonstrator is presented, which considers RSS beamforming with four antenna elements at a Node B of LCR-TDD of UMTS, demonstrating the feasibility of implementing RSS beamforming using today's conventional hardware.
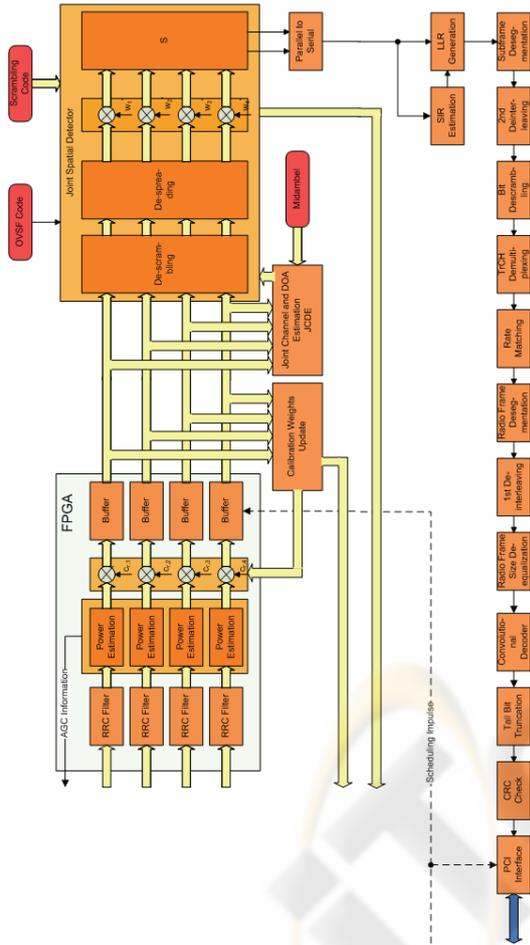

Figure 5: Block diagram for the Node B receiver.

This communication is organized as follows. In Sect. 2, the system model for the channel estimation and the data detection will be presented. Sect. 3 will provide a novel channel estimation and an appropriate data detection algorithm, which are both based on the RSS beamforming concept. In Sect. 4 an implementation concept for a demonstrator will be presented. The performance of the RSS beamforming for the LCR-TDD mode of UMTS will be investigated in terms of simulations in Sect. 5. Both floating-point as well as fixed-point simulation results will be presented. Finally, in

Sect. 6 a conclusion of this communication will be given.

In what follows, the matrix-vector notation is used. Matrices are denoted as upper case characters in bold face italics, vectors are lower case characters in bold face italics. Furthermore, complex-valued variables are underlined. $(\cdot)^{\mathrm{T}}$ and $(\cdot)^{\mathrm{H}}$ denote matrix and vector transposition and complex conjugate transposition of a matrix or a vector.

2 SYSTEM MODEL

In this section, the appropriate system models for channel estimation and data detection are presented. These models assume the LCR-TDD mode of UMTS, where each burst consists of two data parts, data 1 and data 2, separated by a midamble as shown in figure 3. The two data parts hold the user data and consist of 352 chips each. The midamble transmitted in each burst is used for channel estimation and has a length of 144 chips. To mitigate different signal run times within a cell between near and far users each burst is appended by a guard period with a length of 16 chips. The total block length including the guard period is thus 864 chips.

First the system model for the channel estimation is described, which is based on the transmitted midamble. For each user k, $k = 1 \cdots K$ a user specific midamble denoted by the $(L+W-1) \times 1$ vector $\underline{\boldsymbol{m}}^{(k)} = \left(\underline{m}_1^{(k)} \quad \underline{m}_2^{(k)} \quad \cdots \quad \underline{m}_{L+W-1}^{(k)} \right)^{\mathrm{T}}$ is transmitted, where L is the midamble length and W denotes the number of paths. According to the RSS beamforming concept (Seebens et al., 2004), (Scholand et al., 2004) for user k there are N_{b} predetermined directions, into which beams are steered. The array may receive midamble signals by all beams. The channel impulse response associated with each beam is termed Directional Channel Impulse Response (DCIR) and is denoted by the $W \times 1$ vector $\underline{\boldsymbol{h}}_{\mathrm{d}}^{(k,k_{\mathrm{d}})} = \left(\underline{h}_{\mathrm{d},1}^{(k,k_{\mathrm{d}})} \quad \underline{h}_{\mathrm{d},2}^{(k,k_{\mathrm{d}})} \quad \cdots \quad \underline{h}_{\mathrm{d},W}^{(k,k_{\mathrm{d}})} \right)^{\mathrm{T}}$ for the user k, $k = 1 \ldots K$ and for the direction k_{d}, $k_{\mathrm{d}} = 1 \ldots N_{\mathrm{b}}$. Arranging these user and direction specific DCIR for all users in a new vector one obtains the direction specific DCIR vector given by the $KW \times 1$ vector $\underline{\boldsymbol{h}}_{\mathrm{d}}^{(k_{\mathrm{d}})} = \left(\underline{\boldsymbol{h}}_{\mathrm{d}}^{(1,k_{\mathrm{d}})\mathrm{T}} \quad \underline{\boldsymbol{h}}_{\mathrm{d}}^{(2,k_{\mathrm{d}})\mathrm{T}} \quad \cdots \quad \underline{\boldsymbol{h}}_{\mathrm{d}}^{(K,k_{\mathrm{d}})\mathrm{T}} \right)^{\mathrm{T}}$ for direction k_{d}.

The arrangement of the direction specific DCIR vectors associated with all directions in a new vector

leads to the $KN_bW \times 1$ vector $\underline{\boldsymbol{h}}_d = \left(\underline{\boldsymbol{h}}_d^{(1)\mathrm{T}} \quad \underline{\boldsymbol{h}}_d^{(2)\mathrm{T}} \quad \cdots \quad \underline{\boldsymbol{h}}_d^{(N_b)\mathrm{T}} \right)^{\mathrm{T}}$, which is termed the combined DCIR vector.

With the $KW \times KW$ phase rotation matrix for antenna element k_a and direction k_d

$$\underline{\boldsymbol{A}}_s^{(k_a,k_d)} = \begin{pmatrix} \underline{b}_s^{(1,k_a,k_d)}\boldsymbol{I}_W & \boldsymbol{0} & \cdots & \boldsymbol{0} \\ \boldsymbol{0} & \underline{b}_s^{(2,k_a,k_d)}\boldsymbol{I}_W & \cdots & \boldsymbol{0} \\ \vdots & \vdots & \ddots & \vdots \\ \boldsymbol{0} & \boldsymbol{0} & \cdots & \underline{b}_s^{(K,k_a,k_d)}\boldsymbol{I}_W \end{pmatrix}, \quad (1)$$

which contains phase factors associated with antenna element k_a and direction k_d, we define the phase rotation matrix for all antenna elements and all directions by the $KK_aW \times KN_bW$ matrix

$$\underline{\boldsymbol{A}}_s = \begin{pmatrix} \underline{\boldsymbol{A}}_s^{(1,1)} & \underline{\boldsymbol{A}}_s^{(1,2)} & \cdots & \underline{\boldsymbol{A}}_s^{(1,N_b)} \\ \underline{\boldsymbol{A}}_s^{(2,1)} & \underline{\boldsymbol{A}}_s^{(2,2)} & \cdots & \underline{\boldsymbol{A}}_s^{(2,N_b)} \\ \vdots & \vdots & \ddots & \vdots \\ \underline{\boldsymbol{A}}_s^{(K_a,1)} & \underline{\boldsymbol{A}}_s^{(K_a,2)} & \cdots & \underline{\boldsymbol{A}}_s^{(K_a,N_b)} \end{pmatrix}. \quad (2)$$

With the $L \times KW$ matrix of the user specific midamble training sequences $\underline{\boldsymbol{G}}$ (Steiner and Jung, 1994), the $KK_aW \times 1$ received midamble vector $\underline{\boldsymbol{e}}_m$ can be expressed by

$$\underline{\boldsymbol{e}}_m = \left(\boldsymbol{I}_{K_a} \otimes \underline{\boldsymbol{G}} \right) \underline{\boldsymbol{A}}_s \underline{\boldsymbol{h}}_d + \underline{\boldsymbol{n}}_m , \quad (3)$$

where the $KK_aW \times 1$ vector $\underline{\boldsymbol{n}}_m$ models additive noise associated with the received midamble and $\otimes$ is the Kronecker product. The system equation in (3) is the basis for the channel estimation.

For derivation of the system model for data detection we set out from the data parts. In what follows the $N \times 1$ data vector $\underline{\boldsymbol{d}}^{(k)} = \left(\underline{d}_1^{(k)} \quad \underline{d}_2^{(k)} \quad \cdots \quad \underline{d}_N^{(k)} \right)^{\mathrm{T}}$ with a total of N data symbols represents either the first or the second data part of the burst for each user k, $k = 1 \cdots K$. According to (Seebens et al., 2005) the spreading of the data symbols by an Orthogonal Variable Spreading Factor (OVSF) code and the transmission over the directional channel can be expressed by the $N_b(NQ+W-1) \times N$ directional system matrix (Lu, 2002)

$$\underline{\boldsymbol{A}}_d^{(k)} = \underline{\boldsymbol{H}}_d^{(k)} \underline{\boldsymbol{C}}^{(k)}, \quad k = 1 \cdots K . \quad (4)$$

The $N_b(NQ+W-1) \times NQ$ matrix $\underline{\boldsymbol{H}}_d^{(k)}$ describes the transmission over the directional channel and the $NQ \times N$ matrix $\underline{\boldsymbol{C}}^{(k)}$ performs the spreading of the data symbols by applying the OVSF code.

The arrangement of the individual data vectors $\underline{\boldsymbol{d}}^{(k)}$ of all users in a new vector yields the $KN \times 1$ overall

data vector $\underline{\boldsymbol{d}} = \left(\underline{\boldsymbol{d}}^{(1)\mathrm{T}} \quad \underline{\boldsymbol{d}}^{(2)\mathrm{T}} \quad \cdots \quad \underline{\boldsymbol{d}}^{(2)\mathrm{T}} \right)^{\mathrm{T}}$. According to (Seebens et al., 2005) the system equation for detection of the data transmitted in one of the data parts of a specific burst is given by

$$\underline{\boldsymbol{e}}_d = \left(\underline{\boldsymbol{B}}_s \otimes \boldsymbol{I}_{NQ+W-1} \right) \underline{\boldsymbol{A}}_d \underline{\boldsymbol{d}} + \underline{\boldsymbol{n}}_d . \quad (5)$$

The $K_a(NQ+W-1) \times 1$ vector $\underline{\boldsymbol{e}}_d$ in (5) represents the received data vector and the $K_a(NQ+W-1) \times 1$ vector $\underline{\boldsymbol{n}}_d$ is additive noise associated with the received data. The $KN_b(NQ+W-1) \times KN$ matrix $\underline{\boldsymbol{A}}_d$ is the overall directional system matrix and is composed of directional system matrices for individual users $\underline{\boldsymbol{A}}_d^{(k)}$, $k = 1 \cdots K$ (Seebens et al., 2005). The $K_a \times KN_b$ combined steering matrix $\underline{\boldsymbol{B}}_s$ is composed of steering matrices for the individual users $\underline{\boldsymbol{B}}_s^{(k)}$, $k = 1 \cdots K$ (Seebens et al., 2005). The bases of the $K_a \times N_b$ steering matrices $\underline{\boldsymbol{B}}_s^{(k)}$ for user k are the $K_a \times 1$ steering vectors $\boldsymbol{b}_s^{(k,k_d)}$ for the predetermined beams (Godara, 1997). The system equation (5) is used to derive the estimation matrix of the Spatio-Temporal Zero-Forcing Block Linear Equalizer (ST-ZF-BLE) (Seebens et al., 2005).

3 CHANNEL ESTIMATION AND DATA DETECTION USING THE RSS BEAMFORMING

Setting out from the system equation (3) the maximum likelihood (ML) estimate of the $KN_bW \times 1$ combined DCIR vector $\hat{\underline{\boldsymbol{h}}}_d$ can be expressed as follows

$$\hat{\underline{\boldsymbol{h}}}_d = \left[\underline{\boldsymbol{A}}_s^{\mathrm{H}} \left(\boldsymbol{I}_{K_a} \otimes \underline{\boldsymbol{G}}^{\mathrm{H}} \right) \underline{\boldsymbol{R}}_{n_m}^{-1} \left(\boldsymbol{I}_{K_a} \otimes \underline{\boldsymbol{G}} \right) \underline{\boldsymbol{A}}_s \right]^{-1} \underline{\boldsymbol{A}}_s^{\mathrm{H}} \left(\boldsymbol{I}_{K_a} \otimes \underline{\boldsymbol{G}}^{\mathrm{H}} \right) \underline{\boldsymbol{R}}_{n_m}^{-1} \underline{\boldsymbol{e}}_m . \quad (6)$$

The $KK_aW \times KK_aW$ covariance matrix of the noise $\underline{\boldsymbol{R}}_{n_m}$ associated with the received midamble, owing to the spatio-temporal equalizer, consists of two components and can be written as

$$\underline{\boldsymbol{R}}_{n_m} = \underline{\boldsymbol{R}}_{\mathrm{DOA}} \otimes \tilde{\underline{\boldsymbol{R}}}_m + N_0 \boldsymbol{I}_{K_a} \otimes \tilde{\underline{\boldsymbol{R}}}_{\mathrm{th,m}} \\ \approx \left[\underline{\boldsymbol{R}}_{\mathrm{DOA}} + N_0 \boldsymbol{I}_{K_a} \right] \otimes \tilde{\underline{\boldsymbol{R}}}_m . \quad (7)$$

The first Kronecker product in (7) takes the spatial component into account, where the $K_a \times K_a$ matrix $\underline{\boldsymbol{R}}_{\mathrm{DOA}}$ is the spatial covariance matrix and the $KW \times KW$ matrix $\tilde{\underline{\boldsymbol{R}}}_m$ is the temporal covariance matrix of the interferers associated with the received midamble, thus representing the spectral form of the interfering signals. The second Kronecker product

denotes the thermal noise with the $KW \times KW$ matrix $\underline{\tilde{R}}_{\mathrm{th,m}}$ being the normalized temporal covariance matrix of the colored noise and N_0 being the spectral noise density. The approximation in (7) is owed to the assumption that $\underline{\tilde{R}}_{\mathrm{m}}$ is approximately identical to $\underline{\tilde{R}}_{\mathrm{th,m}}$.

Using (7) and writing the received midambles in a $KW \times K_{\mathrm{a}}$ matrix as

$$\underline{E}_{\mathrm{m}} = \left(\underline{e}_{\mathrm{m}}^{(1)} \quad \underline{e}_{\mathrm{m}}^{(2)} \quad \cdots \quad \underline{e}_{\mathrm{m}}^{(K_{\mathrm{a}})} \right), \qquad (8)$$

we can rewrite (6) as

$$\underline{\hat{h}}_{\mathrm{a}} \approx \mathrm{vec}\left\{ \left(\left(\underline{G}^{\mathrm{H}} \underline{\tilde{R}}^{-1} \underline{G} \right)^{-1} \underline{G}^{\mathrm{H}} \underline{\tilde{R}}_{\mathrm{m}}^{-1} \right) \underline{E}_{\mathrm{m}} \left[\underline{R}_{\mathrm{DOA}}^{*} + N_0 \underline{I}_{K_{\mathrm{a}}} \right]^{-1} \underline{B}_{\mathrm{s}}^{*} \right) \left(\underline{B}_{\mathrm{s}}^{\mathrm{T}} \left[\underline{R}_{\mathrm{DOA}}^{*} + N_0 \underline{I}_{K_{\mathrm{a}}} \right]^{-1} \underline{B}_{\mathrm{s}}^{*} \right)^{-1} \right\}. \qquad (9)$$

In this equation the operator $\mathrm{vec}\{\cdot\}$ stacks the columns of the matrix.

To determine the data detector we set out from the system equation (5). The ML estimate of the $KN \times 1$ data vector $\underline{\hat{d}}$ is then given by (Seebens et al., 2005)

$$\underline{\hat{d}} = \left[\underline{A}_{\mathrm{d}}^{\mathrm{H}} \left(\underline{B}_{\mathrm{s}}^{\mathrm{H}} \otimes \underline{I}_{NQ+W-1} \right) \underline{R}_{n_{\mathrm{d}}}^{-1} \left(\underline{B}_{\mathrm{s}} \otimes \underline{I}_{NQ+W-1} \right) \underline{A}_{\mathrm{d}} \right]^{-1} \underline{A}_{\mathrm{d}}^{\mathrm{H}} \left(\underline{B}_{\mathrm{s}}^{\mathrm{H}} \otimes \underline{I}_{NQ+W-1} \right) \underline{R}_{n_{\mathrm{d}}}^{-1} \underline{e}_{\mathrm{d}}$$
$$. \qquad (10)$$

In accordance to (7) the $K_{\mathrm{a}}(NQ+W-1) \times K_{\mathrm{a}}(NQ+W-1)$ covariance matrix of the noise $\underline{R}_{n_{\mathrm{d}}}$ associated with the received data can be approximated as

$$\underline{R}_{n_{\mathrm{d}}} \approx \left[\underline{R}_{\mathrm{DOA}} + N_0 \underline{I}_{K_{\mathrm{a}}} \right] \otimes \underline{\tilde{R}}_{\mathrm{d}}, \qquad (11)$$

where the $(NQ+W-1) \times (NQ+W-1)$ matrix $\underline{\tilde{R}}_{\mathrm{d}}$ is the temporal covariance matrix of the interferers associated with the received data. A comparison of (7) with (11) yields, that the covariance matrices $\underline{R}_{n_{\mathrm{m}}}$ and $\underline{R}_{n_{\mathrm{d}}}$ have the same properties. Note, however, that these matrices have different dimensions, because the midamble and the data parts have different dimensions.

Writing the received data symbols in a $(NQ+W-1) \times K_{\mathrm{a}}$ matrix as

$$\underline{E}_{\mathrm{d}} = \left(\underline{e}_{\mathrm{d}}^{(1)} \quad \underline{e}_{\mathrm{d}}^{(2)} \quad \cdots \quad \underline{e}_{\mathrm{d}}^{(K_{\mathrm{a}})} \right), \qquad (12)$$

one can rewrite (10) by using (11) as (Seebens et al., 2005)

$$\underline{\hat{d}} \approx \left[\underline{A}^{\mathrm{H}} \left[\underline{R}_{\mathrm{DOA}} + N_0 \underline{I}_{K_{\mathrm{a}}} \right]^{-1} \otimes \underline{\tilde{R}}_{\mathrm{d}}^{-1} \underline{A} \right]^{-1} \underline{A}_{\mathrm{d}}^{\mathrm{H}} \mathrm{vec}\left\{ \underline{\tilde{R}}_{\mathrm{d}}^{-1} \underline{E}_{\mathrm{d}} \left[\underline{R}_{\mathrm{DOA}}^{*} + N_0 \underline{I}_{K_{\mathrm{a}}} \right]^{-1} \underline{B}_{\mathrm{s}}^{*} \right\}$$
$$. \qquad (13)$$

In (13) the beamforming can be identified as being carried out by the matrix product $\left[\underline{R}_{\mathrm{DOA}}^{*} + N_0 \underline{I}_{K_{\mathrm{a}}} \right]^{-1} \underline{B}_{\mathrm{s}}^{*}$. Since the matrix $\underline{B}_{s}$ is composed of the steering vectors $\underline{b}_{\mathrm{s}}^{(k,k_{\mathrm{d}})}$, the optimal beamforming weights can be written by $K_{\mathrm{a}} \times 1$ vectors (Seebens et al., 2005)

$$\underline{w}_{\mathrm{opt}}^{(k,k_{\mathrm{d}})} = \left[\underline{R}_{\mathrm{DOA}}^{*} + N_0 \underline{I}_{K_{\mathrm{a}}} \right]^{-1} \underline{b}_{\mathrm{s}}^{(k,k_{\mathrm{d}})}, \quad k=1\cdots K, \, k_{\mathrm{d}}=1\cdots N_{\mathrm{b}}. \qquad (14)$$

4 IMPLEMENTATION CONCEPT

To allow the investigation of the performance of RSS beamforming in a real environment, an implementation concept for a demonstrator is presented, which considers RSS beamforming with four antenna elements at a Node B of LCR-TDD of UMTS. For demonstration purposes only simple speech transmission is considered. The User Equipment (UE) is assumed to have a single antenna element, hence modeling a standard LCR-TDD transceiver. This communication concentrates on the implementation of the Node B, since this is considered to be interesting for RSS beamforming in first place. In order to determine the required functions to implement in the Node B, block diagrams for the Node B transmitter and receiver are established.

The block diagram for the Node B transmitter is given in figure 4. The speech data coming from the PCI interface are first processed in a standard way as described in (3GPP TS 25.222 V5.2.0, 2002), (3GPP TS 25.223 V5.1.0, 2002). The subframes generated by the subframe assembler are multiplied with the beamforming weights $\underline{w}_{k_{\mathrm{a}}}$, $k_{\mathrm{a}}=1\cdots4$, which have been generated by the receiver for the previous burst. These weights are used to generate the desired radiation pattern in transmit direction. In order to overcome inhomogeneities in the transmit paths the signals are also subject to calibration by applying calibration weights $\underline{c}_{\mathrm{r},k_{\mathrm{a}}}$ prior to RRC filtering. Then the signals are passed to the RF (Radio Frequency) frontend and radiated by the antenna elements.

The block diagram of the Node B receiver is shown in figure 5. The signals coming from the RF frontends are calibrated by appropriate calibration weights $\underline{c}_{\mathrm{r},k_{\mathrm{a}}}$, $k_{\mathrm{a}}=1\cdots4$ after RRC filtering. The calibration weights are determined from the previous burst and updated with each burst. The calibrated signals are used for channel estimation and data detection. For channel estimation the Joint Channel and DOA Estimation (JCDE) block is responsible. This block determines the DCIR and provides it to the Joint Spatial Detector (JSD). With the help of the DCIR the JSD detects the transmitted data symbols and determines also the beamforming weights. These are transferred to the transmitter. The detected symbols are used to generate Log

Likelihood Ratios (LLR), which are used for the further signal processing according to (3GPP TS 25.222 V5.2.0, 2002), (3GPP TS 25.223 V5.1.0, 2002).

For the digital baseband signal processing Harrier boards from MangoDSP are considered for the Node B as well as for the UE. Each Harrier board provides 15 TI C6416 DSPs (Digital Signal Processor), five Altera Stratix FPGAs (Field Programmable Gate Array), four MangoLink connectors, and a PCI interface. The 15 DSPs are arranged in five clusters with three DSPs each. Each DSP cluster is associated with an FPGA. The FPGAs may be used for digital signal processing, which requires simple operations at high sample rates. The FPGAs can also be programmed to connect the DSPs with each other. Furthermore, the FPGAs are required for operating the MangoLink connectors. There is also a hierarchical system of PCI busses. These allow the DSPs to communicate with each other and with any device attached to the external PCI interface.

Figure 6 shows the board diagram of the Node B. The heart of the Node B are two Harrier boards, one for the transmitter and one for the receiver, respectively. Each of these Harrier boards is connected with the two RF boards, which provide the RF frontend for two antenna elements each. There is an additional RF board which is used to operate a single calibration antenna element, which is required to calibrate the receive paths of the four RF frontends. The board named "Local Oscillator" is used to provide a system wide stable clock which is required for the exact timing.
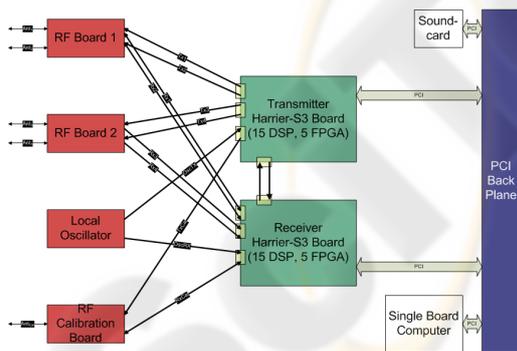

Figure 6: Board diagram for the Node B.

Figure 6 shows the board diagram of the Node B. The heart of the Node B are two Harrier boards, one for the transmitter and one for the receiver, respectively. Each of these Harrier boards is connected with the two RF boards, which provide the RF frontend for two antenna elements each.

There is an additional RF board which is used to operate a single calibration antenna element, which is required to calibrate the receive paths of the four RF frontends. The board named "Local Oscillator" is used to provide a system wide stable clock which is required for the exact timing.

The total system is implemented in a 19" rack which also has a PCI backplane. Besides the two Harrier boards a Single Board Computer (SBC) and a sound card are also attached to the PCI backplane. The SBC is used to control the whole setup and also for the multirate adaptive speech codec, while the sound card is used for speech input and output. However, in order to allow undisturbed real-time communications the Harrier boards are also connected by MangoLinks.
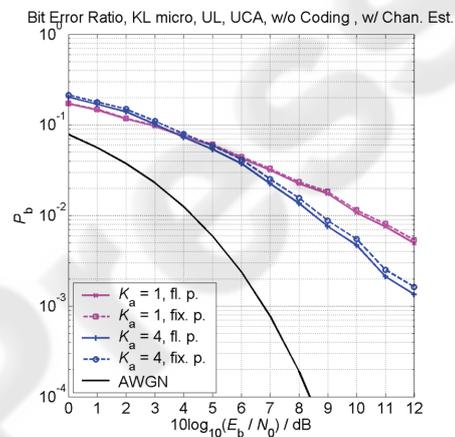

Figure 7: Comparison of the fixed-point implementation with the floating-point implementation.

In order to distribute the identified functions on the DSPs the complexity of each functional block is estimated in terms of Mega Instructions Per Second (MIPS). Implementation guidelines are to implement as many functions on DSPs as possible in order to be as flexible as possible. Hence, only rather simple functions running at high sample rates are implemented on the FPGAs. Moreover, as few as possible DSPs shall be used to keep the overall complexity moderate. Furthermore, the total estimated load of the DSPs shall be below the theoretical maximum of the DSPs keeping a relatively large margin. This analysis reveals that the Node B transmitter can be realized largely on a single DSP. Only the weighting with the calibration and beamforming weights and the RRC filtering is performed in the FPGA. The total load of the DSP is then 8.9526 MIPS (Seebens et al., 2005).

The Node B receiver is much more complex than the

Node B transmitter and requires three DSPs and one FPGA for implementation (Seebens et al., 2005). The FPGA is needed for the RRC filtering and the application of the calibration weights on the received data. Note, that in the Node B receiver, the application of the beamforming weights is performed in the JSD (Seebens et al., 2005). DSP 1 is used for the channel estimation, power estimation, and calculation of the calibration weights. The total load of this DSP with the mentioned functions is estimated to be 61,008 MIPS (Seebens et al., 2005). Since the JSD is the most complex function of the receiver, it requires a DSP more or less on its own. Only minor functions like parallel-to-serial multiplexing, SIR (Signal-to-Interference Ratio) estimation and LLR generation are also located on this DSP. The load of DSP 2 is estimated to be 1583.2884 MIPS (Seebens et al., 2005). The remaining functions according to (3GPP TS 25.222 V5.2.0, 2002), (3GPP TS 25.223 V5.1.0, 2002) are implemented in DSP 3 (Seebens et al., 2005). The total load of this DSP is estimated to be 51.6948 MIPS (Seebens et al., 2005). However, this load can be further reduced by using the internal Viterbi Coprocessor of the TI C6416 DSP.

5 SIMULATION RESULTS

In (Seebens et al., 2004), (Scholand et al., 2004) Matched Filter Bounds (MFB) were simulated to investigate the performance of the RSS beamformer in the uplink transmission direction. MFBs provide a lower limit for the achievable Bit Error Ratio (BER), that one can expect from an algorithm. The respective MFBs were obtained by considering a spatial mobile channel as described in (Scholand et al., 2004), (Blanz and Jung, 1998). In (Seebens et al., 2004), (Scholand et al., 2004) it has been shown, that the RSS beamformer outperforms the conventional beamformer by comparing the MFBs.

A comparison between the MFBs in (Seebens et al., 2004), (Jung, 2004) and link-level simulation results for a microcellular channel model is given in (Seebens et al., 2005). For the link-level simulations, the baseband signal processing according to (3GPP TS 25.222 V5.2.0, 2002), (3GPP TS 25.223 V5.1.0, 2002) was implemented in the UE transmitter. In the Node B receiver the functional blocks for the baseband signal processing were implemented as given in figure 5. Especially, the channel estimation and the data detection were performed by using (9) and (13) with the noise covariance matrices assumed

to be the identity matrices. In (Seebens et al., 2005) it was shown, that the implementation loss for a UCA with $K_a = 4$ antenna elements at a BER of 10^{-3} is about 1.4 dB. This degradation is due to imperfect channel estimation and data detection. It should be noted, that the implementation loss of 1.4 dB is a promising result, since the MFBs represent the best possible performance one can expect.

For the link-level simulations in (Seebens et al., 2005) a floating point implementation of the simulator was considered. According to the selected hardware all functional blocks on the DSPs and FPGAs of the demonstrator have to run in a fixed-point implementation. For further validation, a fixed-point implementation of the simulator is used to find limitations and degradations of the fixed point implementation. The functional blocks realized in fixed point can then be transferred directly to the demonstrator hardware.

Figure 7 depicts a comparison of the fixed-point implementation with the floating-point implementation of the simulator for $K_a = 1, 4$ antenna elements. For the simulations the microcellular channel model in (Scholand et al., 2004), (Blanz and Jung, 1998) was considered. In accordance to the simulations in (Seebens et al., 2005) the uplink transmission was considered, where a single user was placed randomly in the environment for each simulation run. For a given signal to noise ratio $10\log_{10}\left(E_b/N_0\right)$ a total of 1000 simulation runs were considered. At each simulation run 100 bursts as shown in figure 3 were transmitted. With QPSK modulation and a spreading factor of eight a total of 17.6 Mio. bits were transmitted for each signal-to-noise value. For the fixed-point implementation a 16 bit quantization was used. This means that the input and the output of each arithmetic operation are fixed-point values with a word length of 16 bit. However, intermediate results may require more bits and have to be scaled appropriately.

In figure 7 the abbreviations "fl. p." and "fix. p." stand for floating point and fixed point, respectively, distinguished by solid and dashed lines. The violet and the blue curves represent the BER for $K_a = 1$ and $K_a = 4$ antenna elements, respectively. From figure 7 it can be observed, that the performance of the fixed-point implementation is slightly worse than that of the floating-point implementation for $K_a = 1$ and $K_a = 4$ antenna elements, respectively. For a UCA with $K_a = 4$ antenna elements the performance degradation of the fixed-point implementation with respect to the floating-point implementation at a

BER of 10^{-2} is only about 0.2 dB.

6 CONCLUSIONS

In this communication an overview of a novel low-cost beamforming concept based on regularly spatial sampling of signals is presented. The performance of the RSS beamforming is investigated by means of simulations with respect to the LCR-TDD mode of UMTS. It has been demonstrated, that the RSS beamformer shows promising performance in terms of bit error ratios. Moreover, a robust fixed-point implementation of the RSS beamforming is presented. For further validation of the performance of the RSS beamformer, an implementation concept for a demonstrator is developed in order to show the feasibility of implementing RSS beamforming on today's readily available hardware platforms. It has been shown, that the total digital baseband signal processing in the Node B receiver can be implemented on three standard DSPs.

ACKNOWLEDGEMENTS

REFERENCES

Holma, H.; Toskala, A.: *WCDMA for UMTS*. Second Edition, Chichester: John Wiley & Sons, 2002.

Lehne, P.H.; Pettersen, M.: An Overview of Smart Antenna Technology for Mobile Communications Systems. *IEEE Communication Surveys*, vol. **2** (1999), pp. 2-13.

Correia, L.M.: *Wireless Flexible Personalised Communications*. Chichester: John Wiley & Sons Ltd., 2001.

Paulraj, A.; Roy, R.; Kailath, T.: ESPRIT – a subspace rotation approach to signal parameter estimation. *Proceedings of the IEEE*. vol. **74** (1986), pp. 1044 – 1045.

Seebens, A.; Hessamian-Alinejad, A.; Kim, S.H.; Scholand, T.; Jung, P.: Low-Cost Exploitation of Spatial Diversity – Regular Spatial Sampling (RSS) Beamforming. *COoperation européenne dans le domaine de la recherche Scientifique et Technique (COST) 273*, 11th Meeting of the Management Committee, Duisburg, Germany, 2004.

Scholand, T.; Kim, S. H.; Hessamian-Alinejad, A.; Seebens, A.; Jung, P.: Regular spatial sampling (RSS) beamforming for the low-cost exploitation of spatial diversity. *Proceeedings of the Third IASTED International Conference on Communications, Internet and Information Technology (CIIT 2004)*, St. Thomas, US Virgin Islands, 2004, pp. 437 – 442.

3GPP TS 25.221 V5.2.0 (2002-09): *Physical Channels and Mapping of Transport Channels onto Physical Channels (TDD)*, Release 5, 2002.

Steiner, B.; Jung, P.: Optimum and suboptimum channel estimation for the uplink of CDMA mobile radio systems with joint detection. *European Transactions on Telecommunications (ETT)*, vol. **5** (1994), pp. 39-50.

Seebens, A.; Ann, J.; Hessamian-Alinejad, A.; Burnic, A.; Lee, E.; Scholand, T.; Jung, P.: Performance of RSS Beamforming for TD-SCDMA Transceibvers. *Proceedings of the Third IASTED International Conference on Communications and Computer Networks (CCN 2005)*, Marina del Rey, CA, USA, 2005.

Lu, Y.: *Contributions to the application of adaptive antennas and CDMA code pooling in the TD-CDMA downlink*. Ph.D. Dissertation, Universität Kaiserslautern, (2002), http://kluedo.ub.uni-kl.de/volltexte/2002/1290/pdf/dissertation_7.pdf.

Godara, L. C.: Application of Antenna Arrays to Mobile Communications, Part II: Beam-Forming and Direction-of-Arrival Considerations. *Proceedings of the IEEE*, vol. **85** (1997), pp. 1195 – 1245.

3GPP TS 25.222 V5.2.0: *Technical Specification; Multiplexing and channel coding (TDD)*. Release 5, 2002.

3GPP TS 25.223 V5.1.0: *Technical Specification; Spreading and modulation (TDD)*. Release 5, 2002.

Seebens, A.; Hessamian-Alinejad, A.; Burnic, A.; Jeong, K.Y.; Scholand, T.; Lee, H.W.; Jung, P.: Implementation Concept of a LCR-TDD Node B with RSS Beamforming Capabilities. *Proceedings of the Third IASTED International Conference on Communications and Computer Networks (CCN 2005)*, Marina del Rey, CA, USA, 2005.

Blanz, J. J.; Jung, P.: A flexibly configurable spatial model for mobile radio channels. *IEEE Transactions on Communications*, vol. **46** (1998), pp. 367 – 371.